Proceedings of the ASME 2021 Conference on Smart Materials,
Adaptive Structures and Intelligent Systems
SMASIS2021
September 14-15, 2021, Virtual, Online

SMASIS2021-68224

A NEW ANALYTICAL APPROACH FOR BISTABLE COMPOSITES

Vishrut Deshpande; Oliver Myers, Georges Fadel, and Suyi Li.
Department of Mechanical Engineering, Clemson University
Clemson, South Carolina 29634

ABSTRACT

Structures with adaptive capabilities offer many potentials to achieve future needs in efficiency, reliability, and intelligence. To this end, bistable CFRP (Carbon Fibre Reinforced Polymers) composites with asymmetric fiber layout are a promising concept that has shown shape morphing capabilities that adapt to the changes in the environment such as external forces and moments. This adaptability opens them to endless application potentials, ranging from small micro-switches to large airfoil sections in airplane wings or wind turbine blades. To harness this potential, it is essential to predict these composites' physical shapes and behavior accurately. To this end, Hyer and Dano devised the first analytical model based on the concepts of Classical Lamination Theory, and this model has become the cornerstone of almost all subsequent studies. However, this theory uses Kirchoff's theory of thin plates that are limited by several assumptions. As a result, Hyer's theory can predict the overall shape of these laminates but lacks accuracy. A reason for this model's underperformance is that it ignores the inter-laminar stresses and strains, but such stresses/strains play a vital role in the balance of the overall stress field and are found significantly higher near the free edges. To overcome these fundamental limitations, we propose a new analytical approach by combining the Reissner-Mindlin theory with concepts from the Classical Lamination Theory. This new model introduces in-plane rotations as two additional degrees of freedom. Thus, it has five independent variables compared to only three in Hyer and Dano's model and its derivatives. Hence, we have a more complex but more accurate model. This paper outlines our new analytical approach by 1) introducing these two additional degrees of freedom; 2) selecting appropriate polynomial approximations; 3) formulating inter-laminar stresses that are functions of these added rotations; and 4) incorporating these inter-laminar stresses in the potential energy equation. By comparing this model's prediction with the finite element simulation results, we found the new model slightly under predicts the laminate deformation, but the overall accuracy is promising, as evidenced by high R-squared correlation.

Nomen	clature
α_t	Transformed Vector of thermal coefficients
ε_0	Strain Vector
κ	Curvature Vector
Π	Potential Energy
θ_{x}, θ_{y}	Rotations in x-dir and y-dir
c_i	Unknown constants to be determined
L_x, L_y	Length of the laminate in x-dir and y-dir
M_t	Thermal Moment vector
N_t	Thermal Force vector
S and Q	Compliance and Stiffness Matrix respectively
T	Stiffness Transformation matrix for Material to Spatial
	coordinates
U_0, V_0, W	Displacements in x-dir, y-dir and z-dir.
x, y, z	Spatial Coordinates
CFRP	Carbon Fibre Reinforced Polymer

CFRP Carbon Fibre Reinforced Polymer
CLT Classical Lamination theory
FEA Finite Element Analysis

1 INTRODUCTION

In this ever-changing age of technology, the need for dynamic structures as the foundation for dexterous and efficient

^{*}Address all correspondence to this author: vdeshpa@clemson.edu

systems is rapidly increasing. As the traditional structures (e.g., fixed solar panels, rigid airplane wing panels) are becoming inefficient for future needs, adaptive structures offer many exciting prospects, including bio-inspired structures [1–4], energy harvesting structures [5,6], and mechano-electronic hybrid systems [7–9]. One of the materials that offer such capabilities is CFRPs, which can achieve adaptability using the phenomenon of *bistability* from unsymmetric ply layup.

Bistability, in general, is a phenomenon in which a system has two distinct stable equilibriums without external constraints or aids. For example, the simplest two-ply bistable laminate could be made by adding a 90°layer of unidirectional fiber prepreg over a 0°layer. Once cured, the laminate produces a cylindrical shape, and it can switch to another cylindrical shape anti-symmetric to the first one by any external force. The applications of CFRP bistable composites are an ongoing research area with promising initial attempts [10–15].

To understand the full functionality of the bistable CFRP, it is essential to formulate an analytical model to predict the behavior of these laminates. To this end, we have observed various research efforts, and a prominent and widely followed one is the classical lamination theory in combination with Kirchoff's plate theory. Hyer and Dano first developed this model in their seminal paper [16], where they approximated the shapes of the laminates using constant curvatures formulation. The polynomials used for approximation of strain definition and out-of-plane deformation field had redundant terms whose contributions were minimal. This formulation was improved later in their following paper, predicting the snap-through of the unsymmetrical laminate [17]. In this paper, they approximated the strain fields to be of the second-order polynomials and the out-of-plane displacement consisting only of second-order terms. Due to this, the curvatures, which are the second-order differentials of the outof-plane displacements, are constants. This formulation led to under-prediction of the curvatures and hence, displacements.

Mattioni et al. in their paper [18], used an extension of Hyer et al.'s model [17] for the stable state shape predictions of two-patch $[0^{\circ}/0^{\circ}] - [90^{\circ}/0^{\circ}]$ CFRP bistable laminates. To improve the degree of polynomial estimation for the out-of-plane displacement field, they calculate the curvatures using quadratic terms. Their formulation displayed a good agreement with the FEA results for the selected two-patch CFRP laminate. Many other researchers exploited the analytical model proposed by Hyer et al. For example, Algmuni et al. [19] compared the performance of their model for four-patch laminates with finite element simulations. Other mention-worthy researches [12, 20].

In the following sections of this paper, we discuss the limitations of the current analytical model developed by Hyer and Dano; then we propose a new theory in combination with the existing classical lamination theory; and finally, the results from the new analytical model are compared with the finite element simulations, showing high accuracy.

2 Modelling

We observe that there are certain limitations of the Classical Lamination theory in predicting the deformation characteristics of the laminate. The following sections discuss these limitations and the use of Reissner-Mindlin theory in formulating a new analytical model.

2.1 Limitations of CLT and New Approach

All the current analytical models for predicting the behaviors of bistable laminates are derived from the CLT. It is of our critical concern to understand its principles and underlying assumptions. CLT bases on Kirchoff's plate theory, which has several assumptions directly affecting the out-of-plane displacements calculations and hence, the laminate shape. The first assumption states that the cross-section area normal to the midplane of the laminate remains straight even after deformation. This could be understood from figure 1, the line AD is perpendicular to the mid-plane initially and remains flat after deformation (normal direction given by the red arrow). By this assumption, through-the-thickness deformation is ignored.

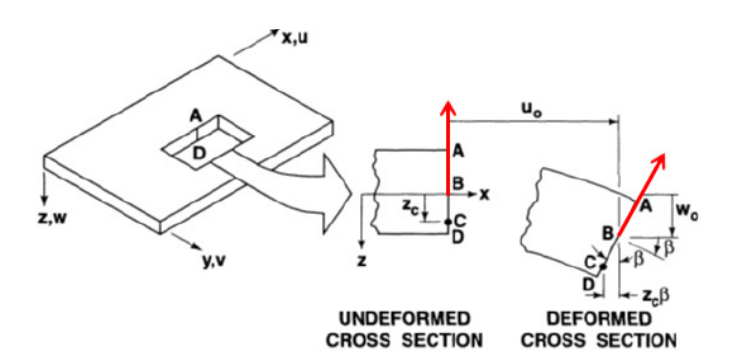


FIGURE 1: Transverse section of the Kirchoff-plate [21]. The red arrow depicts the normal to the mid-plane.

The second assumption states that the slope of the laminate's mid-plane is equal to the rotation angle of the corresponding cross-section area. As observed in the figure, the angle β represents the rotation of the mid-plane axis. Following the above assumption, the cross-section also has a slope equal to β with respect to the vertical reference axis. Therefore, this angle is typically considered small — the in-plane deformations due to this rotation in different laminate layers follow the equation $z*\beta$, where z is the distance between this layer and the mid-plane. This assumption could underestimate laminate deformation, making it appear stiffer than the finite element simulations and experiment results. Also, it is assumed that the laminate thickness does not vary after deformation.

Moreover, due to the above assumptions, the inter-laminar stresses, i.e., stresses in-between the laminate plies, are neglected. Such simplification creates an inconsistency in the stress

field definition. Especially, the stresses appear imbalanced near the free edges of the laminate. Referring to the figure 2, the cut section of the upper ply of the laminate has a free edge surface A-B-C-D. Ideally, the free edges should have zero stress on their surface. However, under the assumptions of CLT, the surface on the x-z plane of the cut section has a shear stress τ_{xy} from the strain definition. To balance it, the other two adjacent surfaces and the surface A-B-C-D must also have a stress τ_{xy} . This indeed violates the free edge condition (i.e., stresses on the surface should be zero due to the absence of external loads). Due to this shear stress on the free edge surface, under-estimation of deflections and over-estimation of frequencies and buckling load have been observed [21].

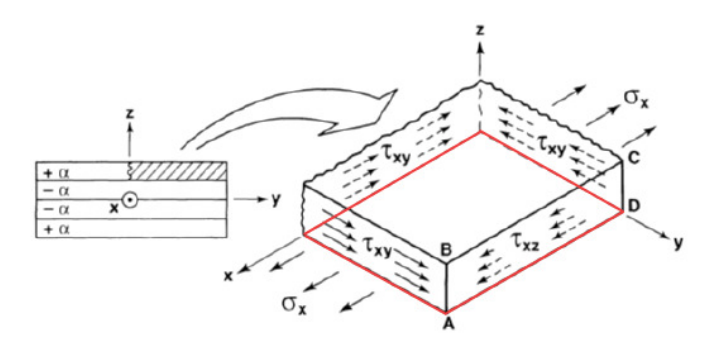


FIGURE 2: The effect of inter-laminar stresses. The red lines emphasize the plane on which inter-laminar stress τ_{xx} acts. [21]

The neglection of inter-laminate stress in the classical lamination theory also makes it incapable of explaining the free-edge delamination failure (aka. separation of fiber plies in the laminate). In reality, inter-laminate stress τ_{xz} acting on the lower surface of the ply (highlighted by the red lines in Figure 2) is responsible for balancing the stress field at the free edge. This inter-laminate stress can become very high near the edges to ensure moment equilibrium about the out-of-plane axis (z-axis here) [21]. These issues give rise to our main objective of addressing these issues by using a more elaborate theory.

Here, We propose to adopt the Reissner-Mindlin theory, which allows the in-plane stress τ_{xy} near the free edges to be balanced by the inter-laminar stresses so that free edge surfaces have no stress acting on them. Reissner-Mindlin theory partially addresses the limitations of the CLT by relaxing the second assumption of Kirchoff's theory. This theory introduces two additional independent parameters, rotation about the y-axis θ_x and rotation about the x-axis θ_y , besides the transverse deflection W_0 . This could be understood from the Figure 3; the cross-section A-B (shown in red-line in the upper part of the figure) is initially straight and normal to the mid-plane of the laminate. After deformation, A'-B' is still straight, but no longer normal to the

mid-plane. Therefore, the rotation about the mid-plane is additional degrees of freedom which should provide a better approximation of the laminate deformation.

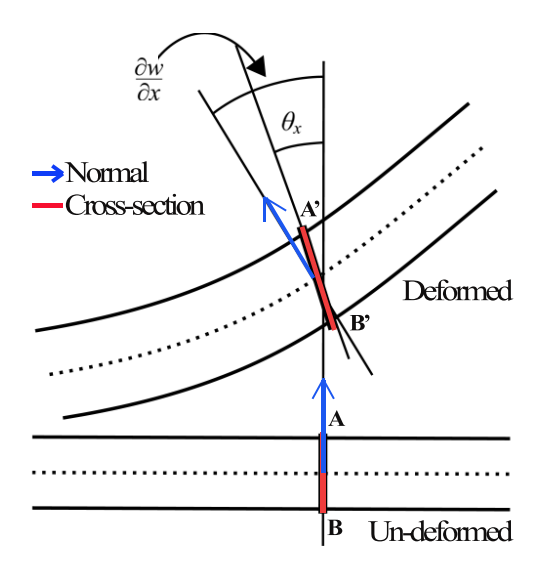


FIGURE 3: Transverse section of the Reissner-Mindlin plate. The normal orientation is shown by the arrow and cross-section by the red-line.

2.2 Formulation based on Reissner-Mindlin Theory

Most of the analytical formulation of the proposed new model is similar to CLT, except for two polynomial approximations for the additional degrees of freedom (rotations θ_x and θ_y) and the two inter-laminar stresses. As a result, the strain and curvature definitions are different from the CLT.

From CLT, the total potential energy of the laminate is a function of the total stiffness of all the plies, the mid-plane strains and curvatures, and the thermal loads and moments. Mathematically, the energy is expressed as follows,

$$\Pi = \int_{-L_{x}/2}^{L_{x}/2} \int_{-L_{y}/2}^{L_{y}/2} \frac{1}{2} \begin{bmatrix} \varepsilon_{0} & \kappa \end{bmatrix} \begin{bmatrix} A & B \\ B & D \end{bmatrix} \begin{bmatrix} \varepsilon_{0} \\ \kappa \end{bmatrix} \\ - \begin{bmatrix} \varepsilon_{0} & \kappa \end{bmatrix} \begin{bmatrix} N_{t} \\ M_{t} \end{bmatrix} dy dx$$
 (1)

In the above equation, the mid-plane strains ε_0 and curvatures κ definitions are adopted from Reissner-Mindlin theory and

modified for our model as,

$$\varepsilon_{0} = \begin{bmatrix} \varepsilon_{x0} \\ \varepsilon_{y0} \\ \gamma_{yz0} \\ \gamma_{xz0} \\ \gamma_{xy0} \end{bmatrix}, \quad \kappa = \begin{bmatrix} \kappa_{x} \\ \kappa_{y} \\ \kappa_{yz} \\ \kappa_{xz} \\ \kappa_{xy} \end{bmatrix} = \begin{bmatrix} -\frac{\partial \theta_{x}}{\partial x} \\ -\frac{\partial \theta_{y}}{\partial y} \\ 0 \\ 0 \\ -(\frac{\partial \theta_{x}}{\partial y} + \frac{\partial \theta_{y}}{\partial x}) \end{bmatrix}. \quad (2)$$

The various terms in the overall stiffness matrix [21] could be calculated using summations as follows,

$$A_{ij} = \sum_{k=1}^{k=n} \overline{Q}_{ij}^{(k)}(z_k - z_{k-1}),$$

$$B_{ij} = \frac{1}{2} \sum_{k=1}^{k=n} \overline{Q}_{ij}^{(k)}(z_k^2 - z_{k-1}^2),$$

$$D_{ij} = \frac{1}{3} \sum_{k=1}^{k=n} \overline{Q}_{ij}^{(k)}(z_k^3 - z_{k-1}^3),$$
(3)

where, N_t is the thermal forces vector induced due to the temperature difference during the laminate curing process, and M_t is a similar thermal moments vector so that

$$N_{t} = \sum_{k=1}^{k=n} \overline{Q}_{ij}^{(k)} \alpha_{t} \nabla T(z_{k} - z_{k-1}),$$

$$M_{t} = \frac{1}{2} \sum_{k=1}^{k=n} \overline{Q}_{ij}^{(k)} \alpha_{t} \nabla T(z_{k}^{2} - z_{k-1}^{2}).$$
(4)

Here, 'n' refers to the number of plies in the laminate. Also, the global stiffness matrix \overline{Q}_{ij} is calculated from the compliance matrix S, which is guided by the orthotropic properties of the fiber ply material. This compliance matrix is defined using the constituent material properties as below,

$$S = \begin{bmatrix} \frac{1}{E_1} & \frac{-\nu_{12}}{E_1} & 0 & 0 & 0\\ \frac{-\nu_{12}}{E_1} & \frac{1}{E_2} & 0 & 0 & 0\\ 0 & 0 & \frac{1}{G_{23}} & 0 & 0\\ 0 & 0 & 0 & \frac{1}{G_{13}} & 0\\ 0 & 0 & 0 & 0 & \frac{1}{G_{12}} \end{bmatrix}$$
 (5)

The relation between the compliance matrix and stiffness matrix is given below. Also, the above compliance matrix is defined in the material coordinate system. The respective values of the material properties are listed in Table 1 and are referred from our previous studies [22]. The transformation of stiffness

TABLE 1: Constituent material properties of Grafil TR50s carbon fibres with Newport 301 resin carbon composite prepregs and thickness = 0.117mm. E_i and G_{ij} are the elastic modulus (unit of GPA). v is the Poisson's ratio. α_{ij} are the thermal coefficients of expansion (unit of ${}^{\circ}C^{-1}$).

Property	Value	Property	Value	Property	Value	
E_1	140	G_{12}	5	α_{11}	-2×10^{-8}	
E_2	9.4	G_{13}	7.17	α_{22}	2.4×10^{-5}	
v_{12}	0.3	G_{23}	3.97	α_{33}	2.4×10^{-5}	

matrix from this material coordinate system to the global coordinate system is,

$$[Q] = [S]^{-1}, \quad [\overline{Q}] = [T][Q][T]^{T}.$$
 (6)

And, the transformation matrix is,

$$T = \begin{bmatrix} \cos^2 \phi & \sin^2 \phi & 0 & 0 & -\sin 2\phi \\ \sin^2 \phi & \cos^2 \phi & 0 & 0 & \sin 2\phi \\ 0 & 0 & 1 & 0 & 0 \\ 0 & 0 & 0 & 1 & 0 \\ \sin \phi \cos \phi - \sin \phi \cos \phi & 0 & 0 & \cos 2\phi \end{bmatrix}. \tag{7}$$

The formulation of the proposed new model involves five independent quantities - mid-plane strain ε_{x0} and ε_{y0} , out-of-plane displacement W_0 , as well as the cross-sectional area rotation θ_x and θ_y . These quantities need to be approximated using appropriate polynomials, and all other quantities are derived from them. Here, we use the approximations by Hyer and Dano [17] for the mid-plane strains ε_{x0} and ε_{y0} so that

$$\varepsilon_{x0} = c_1 + c_2 \frac{x^2}{L_x^2} + c_3 \frac{y^2}{L_y^2} + c_4 \frac{xy}{L_x L_y},$$

$$\varepsilon_{y0} = c_5 + c_6 \frac{x^2}{L_x^2} + c_7 \frac{y^2}{L_y^2} + c_8 \frac{xy}{L_x L_y}.$$
(8)

The most critical assumption here is the out-of-plane displacement field that defines the external shape of the bistable laminate. Hyer and Dano used a constant curvature formulation, so there are only three terms in their W_0 definition [16, 17]. However, we assume a higher-order polynomial for better accuracy. We use a third order-polynomial to define the z-displacement

field:

$$W_{0} = c_{9} \frac{x^{2}}{L_{x}^{2}} + c_{10} \frac{y^{2}}{L_{y}^{2}} + c_{11} \frac{xy}{L_{x}L_{y}} + c_{12} \frac{x^{2}y}{L_{x}^{2}L_{y}} + c_{13} \frac{xy^{2}}{L_{x}L_{y}^{2}} + c_{14} \frac{x^{3}}{L_{x}^{3}} + c_{15} \frac{y^{3}}{L_{y}^{3}},$$

$$(9)$$

And, the cross-section rotations are assumed using the complete second-order polynomials:

$$\theta_{x} = c_{16} \frac{x}{L_{x}} + c_{17} \frac{y}{L_{y}} + c_{18} \frac{xy}{L_{x}L_{y}} + c_{19} \frac{x^{2}}{L_{x}^{2}} + c_{20} \frac{y^{2}}{L_{y}^{2}},$$

$$\theta_{y} = c_{21} \frac{x}{L_{x}} + c_{22} \frac{y}{L_{y}} + c_{23} \frac{xy}{L_{x}L_{y}} + c_{24} \frac{x^{2}}{L_{x}^{2}} + c_{25} \frac{y^{2}}{L_{y}^{2}}.$$
(10)

Based on rotation approximation above, the curvatures, which are the first order differentials of these rotations, are complete first-order polynomials. The in-plane displacements are calculated using the strain definitions as follows,

$$U_{0} = \int \left[\varepsilon_{x0} - \frac{1}{2} \left(\frac{\partial W_{0}}{\partial x} \right)^{2} \right] dx + g(y),$$

$$V_{0} = \int \left[\varepsilon_{y0} - \frac{1}{2} \left(\frac{\partial W_{0}}{\partial y} \right)^{2} \right] dy + h(x).$$
(11)

The in-plane displacements have constants of integration, these are used to complete the polynomials using suitable approximation including the linear and cubic terms as follows,

$$g(y) = g_1 \frac{y}{L_y} + g_2 \frac{y^3}{L_y^3}$$
; $h(x) = h_1 \frac{x}{L_x} + h_2 \frac{x^3}{L_x^3}$. (12)

To eliminate the rigid body rotations in the in-plane displacement field assumption, constraint $g_1 = h_1$ needs to be applied, eliminating one undetermined constant. The in-plane shear is a function of the in-plane and out-of-plane displacement in that

$$\gamma_{xy0} = \frac{\partial U_0}{\partial y} + \frac{\partial V_0}{\partial x} + \frac{\partial W_0}{\partial x} \frac{\partial W_0}{\partial y}.$$
 (13)

Lastly, the inter-laminar shear strains, which are the integral part of our formulation, are calculated as follows,

$$\gamma_{yz0} = \frac{\partial W_0}{\partial y} - \theta_y;
\gamma_{xz0} = \frac{\partial W_0}{\partial x} - \theta_x.$$
(14)

These terms are zero in the CLT formulation due to its assumption that the slope at the cross-section is equal to the midplane rotations. However, in our formulation these terms are a second order polynomials.

The above formulation produces a highly nonlinear equation for the laminate's potential equation, which is a function of the undetermined constants. There are several undetermined constants, 8 from the mid-plane strain definitions, 7 from the out-of-plane displacement field, 10 from the rotations, and 3 from the integration constant. Hence, a total of 28 undetermined constants are used in the new formulation. In comparison, the Hyer's model [16, 17] had only 14 undetermined constants, 3 from the out-of-plane displacement field, 8-from the mid-plane strain definitions, and 3 from the integration constant. Therefore, the analytical model we present is comparatively expensive to compute but is still faster than the FEA simulations.

The solution is achieved by minimization of the potential function 1. To do so, we use MATLAB's built-in multivariate optimizer fmincon, which is designed for highly nonlinear optimization problems. To expedite the calculations, we supply the fmincon solver with the gradients of the potential function with respect to each undetermined constants. Also, all the assumed polynomials are normalized to enhance computation efficiency in that each term is divided by the length size in that direction (either L_x or L_y) of the same order.

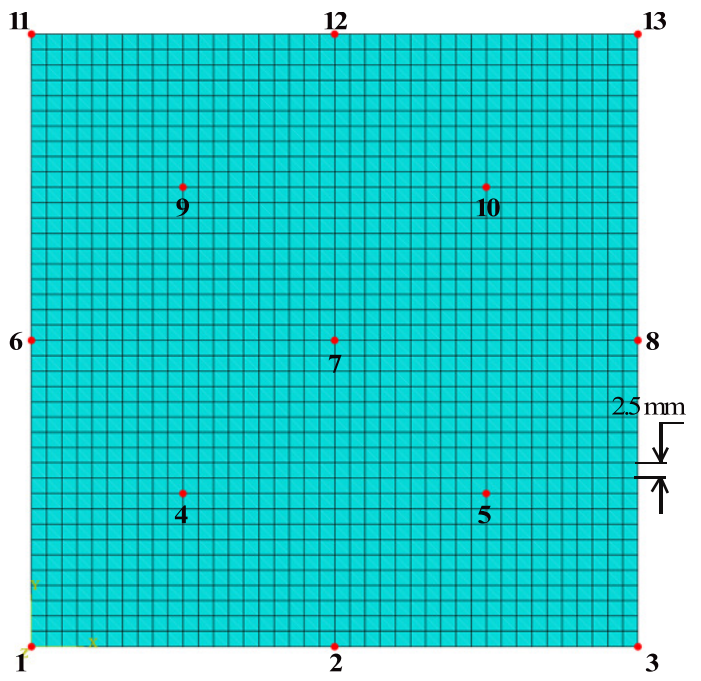


FIGURE 4: FEA model with the mesh size; showing the thirteen selected points whose nodal coordinates are extracted from the simulation results to compare with the analytical model prediction.

2.3 FEA Model

We also modeled the bistable laminates by finite element analysis using ABAQUS 6.14. The "Static Structural" module allows us to model the composite layers based on the patch's ply length, ply thickness, and ply orientation. We have selected to study three types of laminates with different configurations - two-ply laminates with a 100mm×100mm size, fourply laminates of 100mm×100mm, and two-ply laminates with 200×200mm. The material properties used for modeling these CFRP laminates are listed in Table 1. The composite layup model is meshed using S4R elements with a mesh size of 2.5mm (Figure 4). After the completion of modeling, the laminate is cured at the temperature of 135°C in the initial step by fixing all degrees of freedom on the whole laminate, simulating the vacuum bagging procedure. Then, it is cooled down to 20°C (room temperature) with the fixed constraints still applied. This step allows the residual stresses to develop inside the laminate plies as there is a difference in the thermal expansion coefficients in the two in-plane directions. Once settled at room temperature, the laminate is then released of the initial fix of the whole laminate and only the middle node is fixed in U1, U2, U3 and UR3, allowing it to deform into one of the stable shapes freely. For comparison we extract nodal coordinates of thirteen selected points from the final results of the FEA simulation: which are all four corners, the mid-point of every edge, mid-point of all the four quadrants and the center point (Figure 4). These are adequate to capture the overall shape and curvature of the laminates.

3 Results & Observations

To gauge the new model's performance, we compare its predictions of the external shapes of the bistable laminates with different designs and the finite element simulation results. The selected laminate design and comparison parameters are summarized in Table 2. Besides the laminate size and ply number mentioned above, we also test different fiber orientations such as 90° , 60° , 45° , 30° , and 0° . These ply orientations have been widely studied in previous studies; hence their results would be sufficient to justify our model's performance.

Figure 5 shows the two-ply square laminates of $100 \times 100 \text{ mm}^2$ size and different fiber ply orientations. Each of these laminates has a ply of 0° as the base, and the other ply varies in orientation. Four configurations are presented - $[0^\circ/90^\circ], [0^\circ/60^\circ], [0^\circ/45^\circ],$ and $[0^\circ/30^\circ];$ the red dots indicate the the positions of nodal points extracted from the finite element simulations and the numbers 1-13 besides them are in order to indicate the selected points used for comparison. The result shapes from the analytical model are plotted as surfaces, and the *colorbar* shows the range of out-of-plane displacements. Among these results, the maximum deformation occurs in the $[0^\circ/60^\circ]$ laminate at points 3 and 7, which could be attributed to the high twist curvature in the laminate. The $[0^\circ/90^\circ]$ laminate

has almost zero twists in its shape.

We evaluate the discrepancy between our new analytical model predictions and the finite element simulation by comparing the thirteen selected points' displacements. In particular, we quantify the analytical model performance using two measures which helps in holistic comparison. First, a root-mean-squared error (referred to as "R-square" hereafter), which can be calculated as,

R-square =
$$1 - \frac{\sum_{i=1}^{i=13} (p_{\text{act}} - p_{\text{target}})_i^2}{\sum_{i=1}^{i=13} (p_{\text{act}})_i^2},$$
 (15)

where, $p_{\rm act}$ represents the selected nodal position vector in the analytical result, $p_{\rm target}$ refers to the nodal position vector from the FEA simulation results, and i refers to the selected nodes. Here, an R-squared value closer to 1 indicates a better fit, or more accurate model predictions.

Second, a normalized error percentage is determined to compare the the different sized laminates and with different ply thickness. It is calculated from the maximum deviation observed in the results from FEA and analytical result using the extracted points and the max deflection (max z-displacement) observed in the laminate. Mathematically,

normalized error
$$\% = \frac{\text{Max. deviation in Nodes}}{\text{Max. deflection of laminate}} \times 100$$
 (16)

The normalized error helps in comparing the performance of the displacement field function for the changing laminate size and their deformation characteristics defined by the curvatures due to different ply orientations.

Table 2 lists the absolute deviations between the analytical and FEA simulation results at all the selected points, as well as the corresponding R-square value and normalized error percentage. The node 7 has all deviations equal to zero as the the laminate is firstly fixed at the centre in simulations and secondly, the laminate's z-displacement is always zero from the nature of equation 9. We observe the maximum deviation for two-ply laminates (fig. 5) in out-of-plane displacements is 2.2 mm at the two opposite corners (points 3 and 11) in the $[0^{\circ}/45^{\circ}]$ laminate. Even though the maximum deviations in absolute terms are not significant the normalized error suggests otherwise. The maximum of 23.2% error is observed in the $[0^{\circ}/30^{\circ}]$ laminate. Regardless, the R-squared values suggest that the analytical results give an excellent estimation of laminate shapes ($R^2 > 0.95$).

Four-ply laminates are shown in Figure 6. These laminates consist of two plies of 0° and two plies with varying fiber orientations. This result helps in testing our analytical model for stiffer laminates that have smaller deformations. The maximum deviation of 1.3 mm is observed in the 45° laminate. We also observe

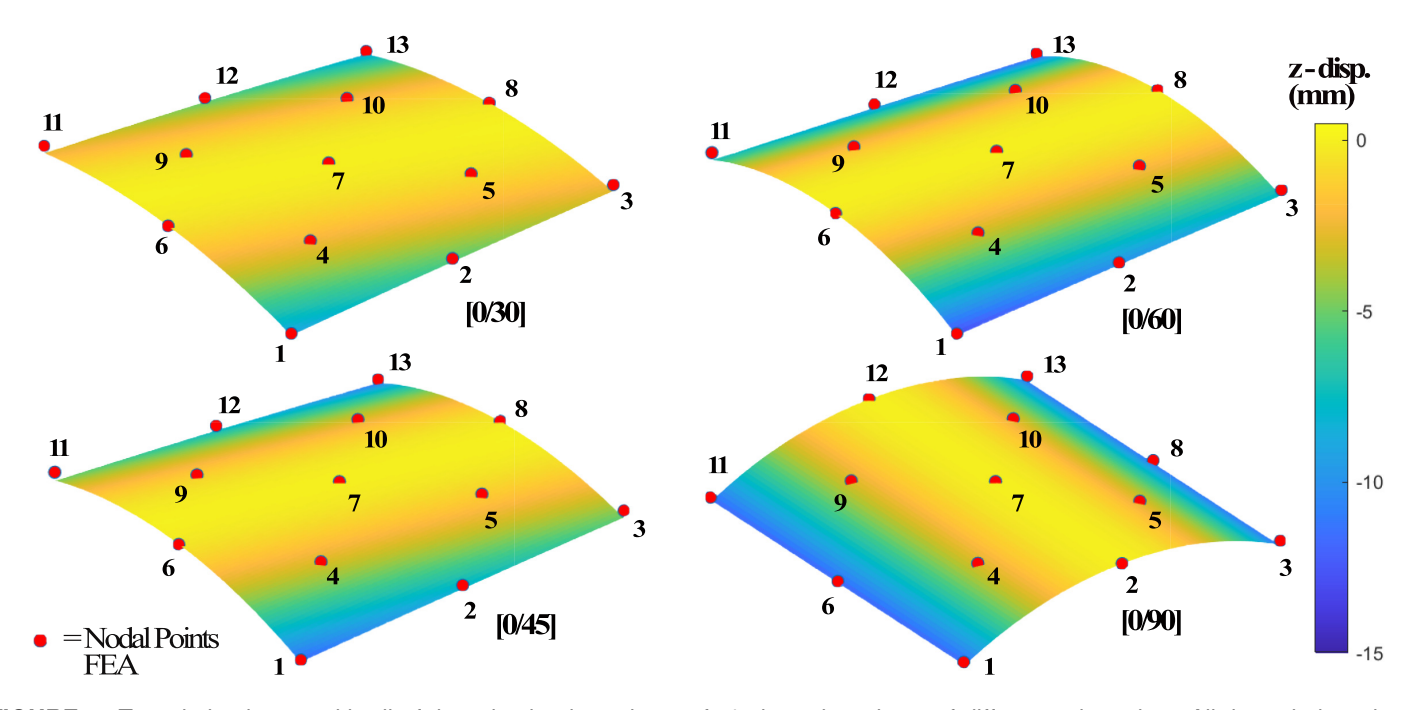


FIGURE 5: Two-ply laminates with all of them having base layer of 0° ply and top layer of different orientation. All the colorbar shows z-displacement values measured in mm.

TABLE 2: Absolute deviation (measured in mm) at the selected points in the result from FEA compared to the analytical model.

Select Points	1	2	3	4	5	6	7	8	9	10	11	12	13	R-sqr. value	Norm. Error
[0°/90°]	1.1	0.1	1.1	0.2	0.2	0.6	0	0.6	0.2	0.2	1.1	0.1	1.1	0.99	10.4
$[0^{\circ}/60^{\circ}]$	0.7	0.8	1.9	0.2	0.4	0.1	0	0.1	0.4	0.2	1.9	0.8	0.7	0.98	16.0
[0°/45°]	0.8	1.2	2.2	0.3	0.4	0.0	0	0.0	0.4	0.3	2.2	1.2	0.8	0.97	20.8
$[0^{\circ}/30^{\circ}]$	0.6	1.0	1.9	0.3	0.3	0.0	0	0.0	0.3	0.3	1.9	1.0	0.6	0.95	23.2
$[0_2^{\circ}/90_2^{\circ}]$	0.6	0.0	0.6	0.0	0.0	0.1	0	0.1	0.0	0.0	0.6	0.0	0.6	0.99	10.5
$[0_2^{\circ}/60_2^{\circ}]$	0.2	0.1	1.2	0.1	0.0	0.1	0	0.1	0.0	0.1	1.2	0.1	0.2	0.98	18.5
$[0_2^\circ/45_2^\circ]$	0.5	0.0	1.3	0.1	0.1	0.1	0	0.1	0.1	0.1	1.3	0.0	0.5	0.96	22.1
$[0_2^\circ/30_2^\circ]$	0.6	0.1	1.2	0.1	0.1	0.0	0	0.0	0.1	0.1	1.2	0.1	0.7	0.91	27.3
[0°/90°] (200mm)	2.5	0.1	2.6	0.1	0.1	2.1	0	2.1	0.1	0.1	2.6	0.1	2.5	0.99	5.8
[0°/60°] (200mm)	1.6	1.0	1.6	0.3	0.1	0.0	0	0.0	0.1	0.3	1.6	1.0	1.6	0.99	3.3
[0°/45°] (200mm)	1.1	0.5	1.1	0.5	0.0	0.1	0	0.1	0.0	0.5	1.1	0.5	1.1	0.99	2.5
[0°/30°] (200mm)	2.1	0.8	0.8	0.6	0.0	0.2	0	0.2	0.0	0.6	0.8	0.8	2.1	0.99	5.6

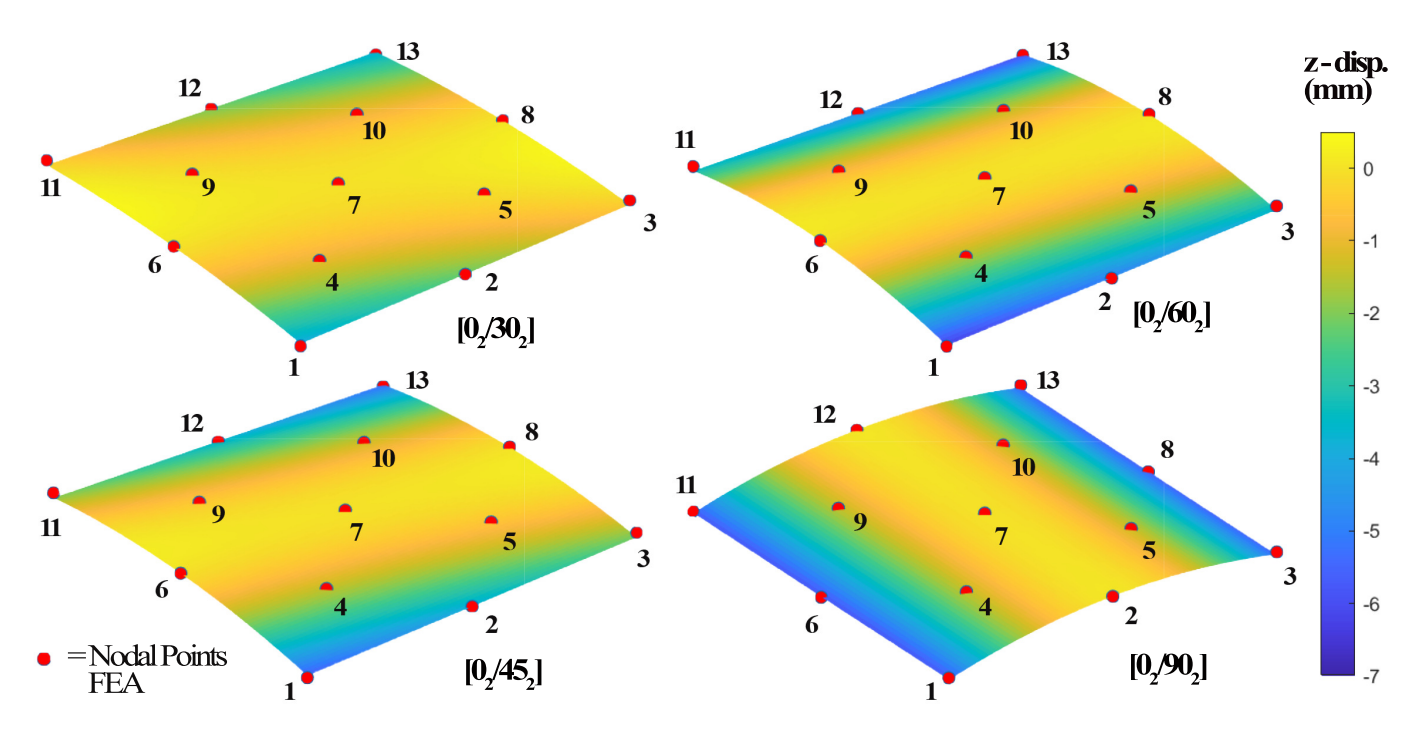


FIGURE 6: Four-ply laminates with all of them having base two layers of 0° ply and top two layers with different orientation. All the colorbar shows z-displacement values measured in *mm*.

that the maximum percentage error is 27.2% for 30° laminate suggesting the relatively poorer performance of our proposed model for this design but, the R-squared values (Row 6-9 in Table 2) are all above 0.91 indicating that the model performs decently for these thick laminates. The performance decreases as the ply orientation changes from 90° to 30°. This drop in performance indicates that our analytical model slightly overestimates the laminate's stiffness and underestimates the deformation. Even though the absolute discrepancy is small, they are not insignificant compared to the total displacements of the selected nodes. Nevertheless, the proposed model still captures the overall laminate shape and could be used for even thicker laminates (with more layers of fiber plies).

Lastly, Figure 7 shows the results for two-ply laminates with a larger dimension, i.e. $200\times200~mm^2$. From rows 10-13 of Table 2, we observe that the max absolute deviations in nodal displacements are similar for these laminates when compared to smaller laminates (rows 2-9); also, R-squared values are all very high (almost close to 1). For example, recall that in the smaller $[0^{\circ}/30^{\circ}]$ laminate in Figure 5, we observe that the maximum deviation in nodal displacement is about 1.9 mm at points 3 and 11. The maximum discrepancy still occurs at points 3 and 11 with a relatively larger (but in the similar range) magnitude of 2.1mm for the larger laminate with the same fiber orientation. However, the R-squared value for the smaller laminate is 0.95 and for the bigger laminate is 0.99. Also, the normalized error has reduced

significantly from 23.2% to 5.6%. This is because a larger laminate also shows a more significant out-of-plane deformation, so the overall ratio between the model discrepancy and the overall deformation becomes smaller. The $[0^{\circ}/45^{\circ}]$ laminate gives the best fit compared to the other configurations but just marginally as it has the lowest normalized error percentage of 2.5%. Overall, the new analytical model performs exceptionally well for all configurations of the two-ply laminates with a bigger size.

4 Conclusion

This study proposes and evaluates a new analytical approach — combining Reissner-Mindlin plate theory and classical lamination theory — to predict the shapes of bistable CFRP laminates. We discuss certain limitations of the currently favored model, initially developed by Hyer and Dano based on Kirchoff's theory, and then attempt to address these limitations by introducing two additional degrees of freedom, i.e., rotations of the laminate cross-section. We conduct case studies using this new model on bistable laminates with "standard" configurations, such as plies at $0^{\circ}, 90^{\circ}, 60^{\circ}, 45^{\circ}, 30^{\circ}$ orientations, square-shaped with 100 mm/200 mm side lengths, and with a two-ply or four-ply construction.

Also, we use finite element simulation to obtain the shapes of the bistable laminates to serve as a basis for the comparison study. We extract nodal positions of thirteen selected points from

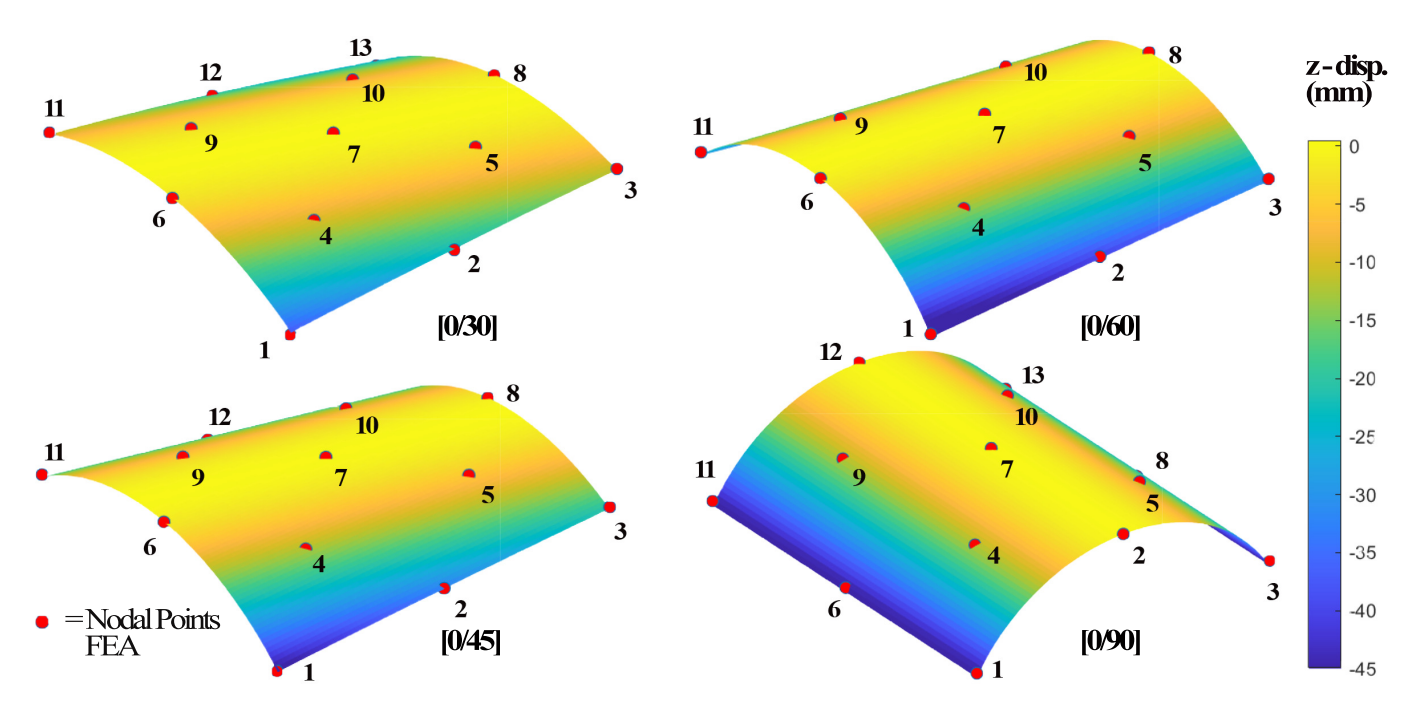


FIGURE 7: Two-ply laminates with all of them having base layer of 0° ply and top layer of different orientation. All the colorbar shows z-displacement values measured in mm.

these simulation results, which are plotted against new analytical model predictions. The absolute deviations between the model prediction and FEA results for all the nodes are summarized and used to calculate the (a) R-squared value for each configuration and, (b) normalized error percentage. The R-squared value serves as a performance indicator of the approximation functions selected for the independent quantities: the mid-plane strains, cross-section rotations about the x and y-axis, and out-of-plane displacement. The closer the R-squared value is to unity, the better the agreement. And, the normalized error percentage compares laminates with different sizes and different deformation characteristics. This also helps in gauging the span of the approximation polynomials used to define the displacement field. These two factors together help in providing a holistic comparison of the FEA results with our analytical model results.

Through comparative studies, we can conclude that the analytical model performs very well over the range of laminate configurations studied. The maximum R-squared values are obtained with bigger laminates with two plies, indicating that the new analytical model is quite accurate for predicting the shapes of the large and thin bistable laminates. The smallest R-squared value and the largest normalized error percentage is observed for a thick $\left[0_2^\circ/30_2^\circ\right]$ four-ply laminate, but the model prediction is still satisfactory for predicting the laminates' shape as the absolute magnitude of deviation is considerably small.

It is worth noting that the accuracy of the shape prediction is hinged mainly on the selection of approximation polynomials for the independent quantities. Hence, for better results, one could use higher-order polynomials, but this would inevitably increase the model's complexity and computational time (but still less than a finite element simulation). Due to the inclusion of the inter-laminar strains in our analytical model, the strain definition is complete. Since, the bistable CFRP laminates are being researched to make active materials by adding passive/active actuators, the inter-laminar interactions of these actuators might have a significant change in the stiffness of the laminate. Thus, the proposed analytical model offers a new angle for such additions to the laminates. In all, we offer a new modeling approach to the composites community, which provides high accuracy in predicting the shapes of bi-stable composites and could serve as a basis for future studies.

Acknowledgement

The authors acknowledge the support from National Science Foundation (CMMI-1760943). S Li also acknowledge the support from Clemson University CECAS Dean's Faculty Fellowship.

REFERENCES

[1] Raman, R., Cvetkovic, C., Uzel, S. G. M., Platt, R. J., Sengupta, P., Kamm, R. D., and Bashir, R., 2016. "Optogenetic skeletal muscle-powered adaptive biological ma-

- chines". Proceedings of the National Academy of Sciences, 113(13), pp. 3497–3502.
- [2] Zhang, Z., Chen, D., Wu, H., Bao, Y., and Chai, G., 2016. "Non-contact magnetic driving bioinspired venus fly-trap robot based on bistable anti-symmetric cfrp structure". *Composite Structures*, *135*, pp. 17 22.
- [3] Elf, J., 2004. "Spontaneous separation of bi-stable biochemical systems into spatial domains of opposite phases". *Systems Biology,* 1, December, pp. 230–236(6).
- [4] Angeli, D., Ferrell Jr, J. E., and Sontag, E. D., 2004. "Detection of multistability, bifurcations, and hysteresis in a large class of biological positive-feedback systems". Proceedings of the National Academy of Sciences of the United States of America, 101(7), feb, pp. 1822–1827.
- [5] Harne, R. L., and Wang, K. W., 2013. "A review of the recent research on vibration energy harvesting via bistable systems". Smart Materials and Structures, 22(2), jan, p. 023001.
- [6] Pellegrini, S. P., Tolou, N., Schenk, M., and Herder, J. L., 2013. "Bistable vibration energy harvesters: A review". *Journal of Intelligent Material Systems and Structures*, **24**(11), pp. 1303–1312.
- [7] Zhang, W., Wang, X., Wang, Y., Yang, G., Gu, C., Zheng, W., Zhang, Y.-M., Li, M., and Zhang, S. X.-A., 2019. "Bio-inspired ultra-high energy efficiency bistable electronic billboard and reader". *Nature Communications*, 10(1), p. 1559.
- [8] Barth, J., Krevet, B., and Kohl, M., 2010. "A bistable shape memory microswitch with high energy density". *Smart Materials and Structures*, *19*(9), aug, p. 094004.
- [9] Wang, G., Cheng, T., Do, Y., Yang, H., Tao, Y., Gu, J., An, B., and Yao, L., 2018. "Printed paper actuator: A low-cost reversible actuation and sensing method for shape changing interfaces". *Conference on Human Factors in Computing Systems Proceedings*, 2018-April (April).
- [10] Daynes, S., and Weaver, P. M., 2012. "A morphing trailing edge device for a wind turbine". *Journal of Intelligent Material Systems and Structures*, 23(6), pp. 691–701.
- [11] Daynes, S., and Weaver, P. M., 2013. "Review of shape-morphing automobile structures: Concepts and outlook". Proceedings of the Institution of Mechanical Engineers, Part D: Journal of Automobile Engineering, 227(11), pp. 1603–1622.
- [12] Udani, J. P., and Arrieta, A. F., 2019. "Analytical Modeling of Multi-sectioned Bi-stable Composites: Stiffness Variability and Embeddability". *Composite Structures*, **216**(November 2018), pp. 228–239.
- [13] Ai, Q., Weaver, P. M., Barlas, T. K., Olsen, A. S., Madsen, H. A., and Andersen, T. L., 2019. "Field testing of morphing flaps on a wind turbine blade using an outdoor rotating rig". *Renewable Energy,* 133, pp. 53–65.
- [14] Emam, S. A., and Inman, D. J., 2015. "A Review on

- Bistable Composite Laminates for Morphing and Energy Harvesting". *Applied Mechanics Reviews*.
- [15] Dai, F., Li, H., and Du, S., 2013. "A multi-stable lattice structure and its snap-through behavior among multiple states". *Composite Structures*, *97*, pp. 56 63.
- [16] Dano, M.-l., and Hyer, M. W., 1998. "Thermally-induced deformation behavior of unsymmetric laminates". *International Journal of Solids and Structures*, *35*(17), pp. 2101–2120.
- [17] Dano, M. L., and Hyer, M. W., 2000. "Snap-through of unsymmetric fiber-reinforced composite laminates". *International Journal of Solids and Structures*, 40(22), pp. 5949–5972.
- [18] Mattioni, F., Weaver, P. M., and Friswell, M. I., 2009. "Multistable composite plates with piecewise variation of lay-up in the planform". *International Journal of Solids and Structures*, **46**(1), pp. 151–164.
- [19] Algmuni, A., Xi, F., and Alighanbari, H., 2020. "Design and analysis of a grid patch multi-stable composite". *Composite Structures*, **246**(January), p. 112378.
- [20] Emam, S. A., 2018. "Snapthrough and free vibration of bistable composite laminates using a simplified Rayleigh-Ritz model". *Composite Structures*, **206**(August), pp. 403–414.
- [21] Jones, R., 1999. *Mechanics Of Composite Materials*. CRC Press. https://doi.org/10.1201/9781498711067.
- [22] Deshpande, V., Myers, O., Fadel, G., and Li, S., 2020. "Transient snap-through of a bistable composite laminate under asymmetric point load". p. 93.